A feasibility study of Organic Rankine Cycle (ORC) power generation using thermal and cryogenic waste energy on board an LNG passenger vessel

Tsougranis, E.-L.; Wu, Dawei

DOI:
10.1002/er.4047

A feasibility study of Organic Rankine Cycle (ORC) power generation using thermal and cryogenic waste energy on board an LNG passenger vessel

Tsougranis, Emmanouil-loizos; Wu, Dawei

DOI:
10.1002/er.4047

A feasibility study of Organic Rankine Cycle (ORC) power generation using thermal and cryogenic waste energy on board an LNG passenger vessel

Emmanouil-Loizos Tsougranis
Newcastle University, School of Marine Science and Technology, Marine Engineering
Newcastle upon Tyne, United Kingdom
e.l.tsougranis@newcastle.ac.uk

Dawei Wu
Newcastle University, School of Marine Science and Technology, Marine Engineering
Newcastle upon Tyne, United Kingdom
dawei.wu@newcastle.ac.uk

***Abstract*— This study develops a novel approach to reutilize cryogenic and thermal waste energy on an LNG powered passenger vessel. The waste energy is identified through a series of field tests of the LNG evaporation system and other important machinery systems, including the main engines, on a case ship. An Organic Rankin Cycle (ORC) power generation system is proposed to work between the LNG boiling temperature of -138°C (at 5 bar) and the waste heat temperature level of 400°C from the main engines' exhaust gas. The proposed ORC system is designed in terms of the field testing data and analyzed through simulation using Siemens LMS Imagine.Lab AMESim. Two different arrangements (single stage and two stages) of ORC are energetically, exergically and economically analysed. Three optimal working fluids are examined in high vacuum and above atmospheric condensing pressures in the temperature range of -110°C to 300°C. The proposed ORC systems are characterized by a significant improvement in thermal efficiency and power production in high vacuum condensing pressures. The two Stage ORC presents higher power output and fuel cost saving per year than the single stage ORC with almost the same payback time. The higher percentage of exergy destruction occurs at the evaporator of the ORC system. The increase in the exergy destruction on the condenser at higher condensing pressures contributes to the decrease of the exergy efficiency of the ORC systems.**

Keywords— LNG cryogenic energy utilization, Organic Rankine Cycle (ORC), Exergetic analysis

NOMENCLATURE

A	Heat transfer area (m^2)
a	Cross flow area (m^2)
B	Baffle spacing (m)
BDC	Bundle diameter clearance (m)
C	Tube clearance (m)
C_{BM}	Bare module cost ($)
C_p	Specific heat capacity (J/KgK)
C_{TM}	Total capital cost ($)
d	Diameter (m)
decC	Degrees Celsius (^oC)
e	Specific exergy (KJ/Kg)
$\dot{E}_D$	Exergy destruction rate (KW)
E_{DR}	Exergy destruction ratio
$\dot{E}_X$	Exergy rate (KW)
f	Friction factor
F_c	Correction factor
FCCS	Ferry consumption cost saving ($)
FCS	Ferry consumption saving (ton/year)
g	Gravity acceleration (m/s^2)
G	Fluid mass velocity (Kg/m^2s)
h	Specific enthalpy (KJ/Kg)
$\dot{H}$	Enthalpy rate (KW)
ID	Inner diameter (m)
k	Thermal conductivity (W/mK)
L	Tube length (m)
LEC	Levelized electricity cost ($\$/KWh$)
$\dot{m}$	Mass flow rate (Kg/s)
Nu	Nusselt number
OD	Outer diameter (m)
P	Pressure (bar)
P_T	Pitch size (m)
PT	Payback time (year)
Pv	Prandle number
$\dot{Q}$	Heat transfer rate (KW)
Re	Reynolds number
R_f	Fouling factor
s	Specific entropy (KJ/KgK)
SIC	Specific investment cost ($/KW)
T	Temperature (^oC)
u	Fluid velocity (m/s)
U	Heat transfer coefficient (W/m^2K)
$\dot{V}$	Volumetric flow rate (m^3/s)
$\dot{V}_r$	Volumetric expansion ratio
$\dot{W}$	Work rate (KW)
$\dot{W}_{Net}$	Work net (KW)

GREEK LETTERS

η	Efficiecny
μ	Dynamic viscosity (Ns/m^2)
ρ	Density (Kg/m^3)
Φ	Dynamic viscosity ratio

Xv	Dryness fraction

SUBSCRIPTS

CEPSI	Chemical engineering plant cost index
CRF	Capital recovery factor
HE	Heat Exchanger
LMTD	Log mean temperature difference
OMC	Operating and maintenance cost
S&T	Shell and Tube
SI	System index
SP	Size parameter
WF	Working Fluid

I. INTRODUCTION

Natural gas is a potential alternative fuel for the shipping industry. Recently, large passenger ships have started to use LNG as a fuel due to low emissions and good economy. In a baseline scenario, Lloyd's Register predicts that there will be 653 LNG ships by 2025 (excluding LNG carriers) to cope with ever stringent emission regulations in Emission Controlled Areas (ECAs) and the global emission caps set in MARPOL by IMO (e.g. global sulphur cap from 3.50% to 0.50% by 2020) [1]. Ship Energy efficiency improvement and Emission reduction through Waste heat recovery in conventional (operating with marine diesel engine) vessels is well established with the addition of economizers. Besides, ship economizers, several studies have been conducted for improving the ship waste heat recovery through the Organic Rankine Cycle. The ORC system proposed by Yuksek and Mirmobin, 2015 [2] utilizes the ship's main engine jacket water (80-95ºC) and sea water (10-30ºC) to facilitate evaporation and condensation of the organic working fluid in order to produce grid-quality electric power. At the design condition the ORC system with WF R245fa presents 125 kW gross power output with 6.5% thermal efficiency. A Regenerative ORC is examined by Ahlgren et al., 2015 [3] operating between the ship engine exhaust gas (580K) and an intermediate loop between the heat sink (exhaust gas) and the condenser (sea water at 290K) of the cycle. The ORC power output is 750KW with the WF Benzene and thermal efficiency up to 24%. However, in LNG powered vessels a large amount of LNG is stored in fuel tanks on board (e.g. -138°C at 5 bar) and is evaporated to gaseous form at 27ºC before reaching gas engines. Therefore, except waste thermal recovery the stored LNG offers waste cold energy recovery.

The LNG cold energy recovery for LNG receiving terminals is examined in literature; like the LNG direct expansion cycle in combination with Rankine cycle in three different pressure levels (4, 35 and 150bar) [4] presenting a second low efficiency of 28%. Although cycles operating in high pressure like the supercritical Rankine cycle [5] utilize more thermal energy, often lead to difficulties for contraction, operation and safety.

Moreover, according to Kim et al., 2013 [6] the regenerate ORC power cycle utilizing the low-grade heat source and the LNG cold energy for land base application can reach up to 35% of thermal efficiency without considering the energy losses on the system components and most of the candidate working fluids reach high pressure above 20 bars.

For LNG powered vessels the design and development of a sophisticated system that will utilize the thermodynamic cycle from the highest thermal waste temperature to the lowest cold temperature of LNG needs to be in low evaporation pressure [7]. Furthermore, a regenerative ORC demonstrates higher efficiency than simple ORC for producing the same amount of electricity by releasing less waste heat with lower irreversibility [8]. Hence, this study proposes and analyses a design of ORC with regeneration and 2 stage expander with reheat, that operates below 15 bars pressure and demonstrates thermal efficiency more than 35%; the maximum operating pressure of 15 bars for marine industry is significant because defines the low cost and the ease of construction [7]. Two proposed ORC arrangements are examined through energy, exergy and economic analysis considering the energy losses on the system components.

II. VESSEL OPERATIONAL ANALYSIS

Fig. **1** shows the Dual Fuel (DF) Electric power plant of the vessel. It consist of 4 Dual Fuel engines and 2 LNG tanks of 400m^3.

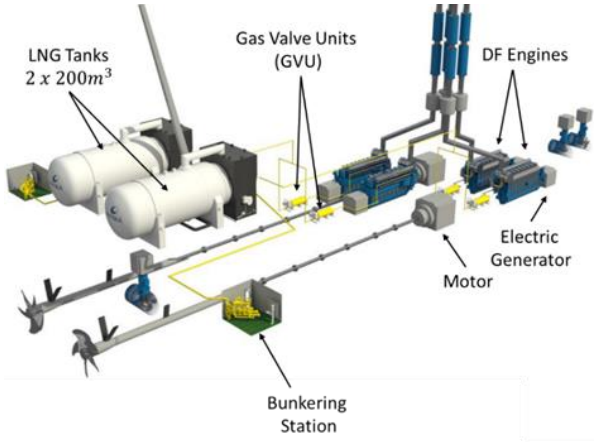

Fig. 1. DF-Electric power plant [9]

Each engine maximum power output is 7.6MW. While the vessel is operated in open sea where the demand of load is at highest capacity only three engines operate at 87% of their power capability. The fourth DF engine is for redundancy.

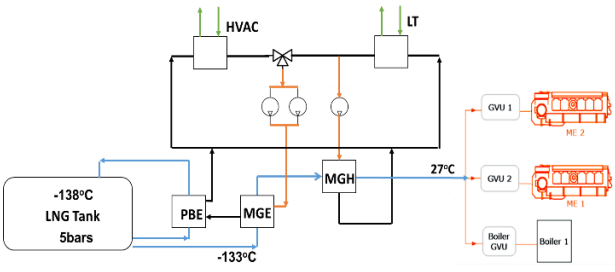

Fig. 2. Fuel gas system for Pack 1 [10]

The Fuel gas system consists of two Packs. Fig. 2 depicts the schematic diagram of Pack 1. The LNG is stored in the tank at -138ºC at 5 bar. The pressure built up evaporator (PBE) maintain the pressure inside the tank at 5bar. The main gas evaporator (MGE) heats up the natural gas (NG) from 133ºC up to 4ºC.

Finally the main gas heater (MGH) heats further up the NG to 27ºC which is the operational temperature of the fluid before enters the Gas Valve Units (GVU). The GVU principle is to stabilize the pressure of the NG at around 3 bars and ensures a quick and reliable shutdown of the gas supply. The current system recovers the LNG cold energy to the HVAC (Heating, Ventilation, Air-Conditioning) and Low Temperature (LT) systems through an intermediate refrigerant. The exergy ($\dot{E}_x$) that is stored in the LNG from the liquefaction process is characterized as:

$$\dot{E}_x=\dot{m}\left((h_s-h_0)+T_0(S_0-S_s)\right) \quad (1)$$

The exergy of the LNG consists of the cold and pressure exergy:

$$\dot{E}_{x\text{-}Cold}=C_p(T_s-T_0)+C_pT_0\ln\frac{T_0}{T_s} \quad (2)$$

$$\dot{E}_{x\text{-}pressure}=RT_0\ln\frac{P_0}{P_s} \quad (3)$$

The system pressure P_s and the dead state temperature T_o are the dominant factors affecting the exergy of LNG and will determine the usage of the LNG cold energy. In TABLE I, the amount of LNG exergy and energy released from MGE and MGH in the fuel gas system in Fig. 2 is estimated when the engines operate in the maximum load mode. It is noticed that the recovery of the LNG cold energy starts at -133ºC. At this temperature, the LNG has already changed phase into vapour. Therefore, the existing fuel gas system actually only utilizes the sensible heat of LNG.

TABLE I. LNG COLD ENERGY AND EXERGY

Heat Exchangers	Energy (KW)	Exergy (KW)
MGE	286.7	106
MGH	46.6	1.5
Total	333.3	107.5

The LNG cold energy between -138ºC to -133ºC is dissipated through the surroundings including the significant amount (471.18 KJ/Kg) of the enthalpy of formation form liquid to vapor phase; at the specific temperature range the LNG cold energy release is 410KW. In particularly, the phase change of the LNG into NG is happening in the pipe directly after the tank, before reaching the MGE HE due to the ambient temperature (288K) difference. Therefore the LNG latent heat of evaporation is getting lost through the pipe walls to the environment. The losses of the current LNG cold energy recovery system are more than 50%.

III. PROPOSED ORC SYSTEM FOR REUTILIZING BOTH CRYOGENIC AND THERMAL ENERGY

The study proposes dual reutilization of the LNG cold and Thermal waste energy of the vessel's power plant through an Organic Rankine Cycle (ORC) system. The ORC is designed to replace the MGE and MGH of the ferry. Specifically, the LNG cold energy is used for the condensation of the ORC working fluid through the cryogenic pump as it is presented in Fig. 3. The LNG reaches the condenser in liquid form so as the latent heat of evaporation to be utilized by the condenser (the phase change of LNG to NG takes place in the condenser). Furthermore, LNG is heated through the condenser up to 27°C, which is the operational temperature of NG before it enters the GVU. The exhaust gas from the DF engines is used as heat source for the evaporator of the ORC. Three working fluids (WF) are examined for the ORC system. Two designs of ORC arrangements are energetically and exergetically analysed for different pressure ratios of the expander when the ferry is operated at the Archipelagos at its optimum speed.

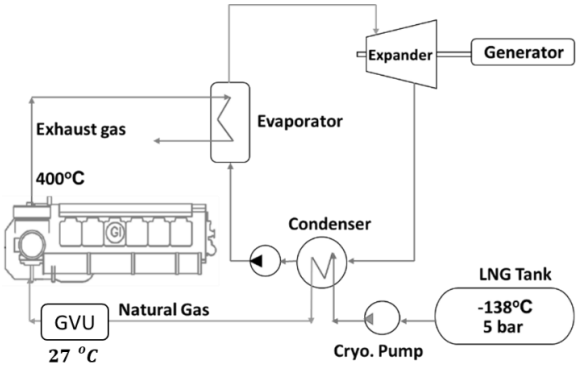

Fig. 3. Proposed ORC arrangement

In maximum voyage speed, three DF engines are running at 87% of load. The respective LNG consumption is 0.875 Kg/s and each engine exhaust gas mass flow rate is 10.44 Kg/s at 400ºC.

A. Working fluid selection

The candidate working fluids need to demonstrate two crucial characteristics, low melting/freezing point below condensation temperatures of -110°C and high thermal stability point above 300°C. The critical temperature, pressure, the boiling point of the WF as well as the environmental impact [Flammability level, Toxicity, Ozone depletion potential (ODP) and Global warming potential (GWP)] are defining criteria for the WF selection. TABLE II present the working fluids properties for Butane (R600), Propane (R290) and Ethylene (C_2H_4) according to Siemens LMS Imagine.Lab AMESim [11]. For modelling purposes LNG is considered to be pure methane CH_4. The exhaust gas is modelled according to the Van der Waals equation.

TABLE II. WORKING FLUIDS CHARACTERISTICS

Working Fluids	P criti. (bar)	T criti. (ºC)	Melting point (ºC)	
R600	38	152	-138	
R290	42.47	96.70	-188	
Ethylene	50.42	9.2	-169	
	Flamm.	**Toxic.**	**ODP**	**GWP**
R600	Yes	No	0	3
R290	Yes	No	0	3
Ethylene	Yes	No	0	4

B. Energetic Analysis

The general energy equation for energy balances at steady state for each component of the system is defined as [12]:

$$\sum \dot{m}_{in} = \sum \dot{m}_{out} \quad (4)$$

$$\dot{Q} - \dot{W} + \sum \dot{m}_{in} h_{in} - \sum \dot{m}_{in} h_{out} = 0 \quad (5)$$

Where, $\dot{Q}$ and $\dot{W}$ represents the heat and work transfer to the surroundings, respectively. The enthalpy rate of the working fluid streams of the system is defined as:

$$\dot{H} = \dot{m}_i h_i \quad (6)$$

The thermal efficiency of the system is given as:

$$\eta_{Thermal} = \frac{\dot{W}_{Net}}{\dot{Q}_{in}} \quad (7)$$

C. Exergetic Analysis

According to the exergy balance steady state [13]:

$$\Sigma \left(1 - \frac{T_0}{T}\right) \dot{Q} - \dot{W} + \sum (\dot{m}_{in} e_{in}) - \sum (\dot{m}_{out} e_{out}) - \dot{E}_d = 0 \quad (8)$$

Where,

- $\left(1 - \frac{T_0}{T}\right) \dot{Q}$ is the exergy transfer by heat transfer to surroundings.
- The exergy transfer due to work is equal to the work ($\dot{W}$) done.
- $\dot{m}_{in} e_{in} - \dot{m}_{out} e_{out}$ is the exergy change of a fluid stream in and out from the system.
- The exergy destroyed ($\dot{E}_d$) is proportional to the entropy generated during the process, $\dot{E}_d = T_0 S_{gen}$.
- T_0 is the dead state temperature while T denotes the temperature at the boundary which heat transfer occurs.

The flow of specific exergy of a stream is given by:

$$e = (h - h_0) - T_0 (s - s_0) + \frac{\overrightarrow{V^2}}{2} + gZ \quad (9)$$

The specific exergy change of the fluid stream as undergoes a process from state 1 to state 2 ignoring the Kinetic and Potential Energy is:

$$\Delta e = e_1 - e_2 = (h_1 - h_2) - T_0 (s_1 - s_2) \quad (10)$$

$\dot{E}_{xi} = \dot{m}_i e_i$ is the exergy rate carried with the flow.

The exergy of the exhaust gas (eg) source to the system is given as:

$$\dot{E}_{xeg} = \dot{m}_{eg} C_{peg} \left(T_{eg} - T_0 - T_0 \ln \frac{T_{eg}}{T_0}\right) \quad (11)$$

While, for the LNG source and the system components the exergy is defined as:

$$\dot{E}_{xi} = \dot{m}_i [(h_i - h_0) - T_0 (s_i - s_0)] \quad (12)$$

The exergy destruction ratio of each component of the system is defined as the exergy destruction on the component over the total fuel exergy supplied to the system [12],

$$E_{DR} = \frac{\dot{E}_d}{\dot{E}_{xin}} \quad (13)$$

The exergy efficiency of the system is expressed as the useful exergy output or the work output of the system over the useful exergy input to the system,

$$\eta_{Ex} = \frac{\dot{W}_{Net}}{\dot{E}_{xin}} = 1 - \frac{\dot{E}_{dtotal}}{\dot{E}_{xin}} \quad (14)$$

The exergy input of the system can be defined also as the sum of the work net and total exergy destruction of the system,

$$\dot{E}_{xin} = \dot{W}_{Net} + \dot{E}_{dtotal} \quad (15)$$

The sum of the total exergy destruction ratios and the exergy efficiency of the system is proportional to unity [12],

$$\eta_{Ex} + \sum E_{DRi} = 1 \quad (16)$$

The sustainability of the system can be estimated through the Sustainability Index (SI), [14]. Higher values of SI indicate better sustainability,

$$SI = \frac{1}{1 - \eta_{Ex}} \quad (17)$$

In the exergy analysis the dead state temperature and pressure are considered to be:

$$T_0 = 288K \,, \; P_0 = 1bar$$

The exergetic and SI analysis is considered only for condensing pressures above dead state pressure.

D. Single stage Regenerative ORC

In Regenerative ORC arrangement in Fig. 4, LNG is expanded to NG from 5 to 6 bar and heated up to 27ºC. For the ORC heat input is considered only the exhaust gas of one DF engine with a mass flow rate of 10.44 Kg/s. A regenerative heat exchanger is used to improve the thermal efficiency of the system. The pressure drop of the ORC components for both arrangements is considered negligible.

The ORC energy balances are:

Evaporator:

$$\eta_{Evap.} = \frac{\dot{m}_{WF}\left(h_5 - h_{2'}\right)}{\dot{m}_{eg} C_{peg} (T_{16} - T_{17})} = 0.8 \quad (18)$$

Condenser:

$$\eta_{Con.} = \frac{\dot{m}_{NG} (h_{14} - h_{11})}{\dot{m}_{WF} (h_{8'} - h_1)} = 0.9 \quad (19)$$

Regenerator:

$$\eta_{Regen.}=\frac{(h_2-h_{2'})}{(h_8-h_{8'})}=0.8 \quad (20)$$

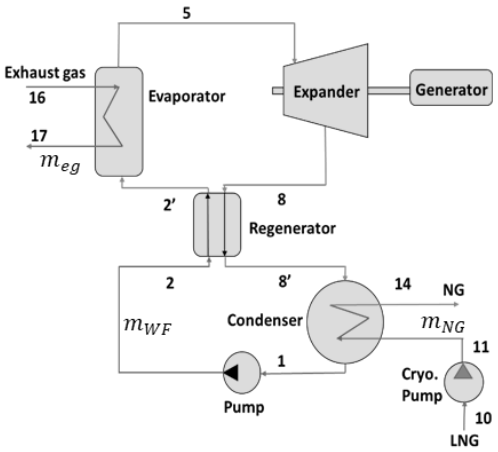

Fig. 4. ORC single stage with Regenerator

The considered isentropic efficiencies of the ORC system assumed lower than of Grljušić etal. [15],

$$\eta_{i\_expander.}=0.83,\ \eta_{i\text{-}pump}=0.65$$

The thermal efficiency of the system is:

$$\eta_{Thermal}=\frac{\dot{W}_{5,8}-\dot{W}_{1,2}-\dot{W}_{10,11}}{\dot{m}_{eg}C_{peg}(T_{16}-T_{17})} \quad (21)$$

The exergy input by the exhaust gas is:

$$\dot{E}_{xeg}=\dot{E}_{x16}-\dot{E}_{x17} \quad (22)$$

The exergy input by the LNG is:

$$\dot{E}_{xLNG}=\dot{E}_{x10}-\dot{E}_{x14} \quad (23)$$

The total exergy input to the system is:

$$\dot{E}_{xin}=\dot{E}_{xeg}+\dot{E}_{xLNG} \quad (24)$$

The exergy destruction on the system components is:

- Evaporator:

$$\dot{E}_{dEva.}=(\dot{E}_{x16}-\dot{E}_{x17})+(\dot{E}_{x2'}-\dot{E}_{x5}) \quad (25)$$

- Expander:

$$\dot{E}_{dExpa.}=\dot{E}_{x5}-(\dot{E}_{x8}+\dot{W}_{5,8}) \quad (26)$$

- Regenerator:

$$\dot{E}_{dRegen.}=(\dot{E}_{x2}-\dot{E}_{x2'})+(\dot{E}_{x8}-\dot{E}_{x8'}) \quad (27)$$

- Pump:

$$\dot{E}_{dPump}=\dot{E}_{x1}+\dot{W}_{1,2}-\dot{E}_{x2} \quad (28)$$

- Condenser:

$$\dot{E}_{dCon.}=(\dot{E}_{x8'}-\dot{E}_{x1})+(\dot{E}_{x11}-\dot{E}_{x14}) \quad (29)$$

- Cryo. Pump:

$$\dot{E}_{dCr.Pump}=\dot{E}_{x10}+\dot{W}_{10,11}-\dot{E}_{x11} \quad (30)$$

E. Two stage Regenerative Reheated ORC with Direct Expansion

This arrangement is characterized by two cycles, the ORC and Direct Expansion Cycle, Fig. 5. The Net-work ($\dot{W}_{Net}$) is a sum of HP, LP and B expanders.

The diversity from the single stage ORC cycle is the WF which after the High pressure (HP) expander is reheated through the evaporator and is expanded again through the Low pressure (LP) expander. Moreover, in the direct expansion cycle, the LNG is pumped from 5 bar at -138ºC into 15 bar, is evaporated through the condenser and finally expanded through the expander B to 5 bar at T_{15}=27ºC. For the Thermodynamic analysis energy balances are considered according to Equations (18), (19), (20), and the isentropic efficiencies assumed as, $\eta_{iExpander}$=0.83, η_{ipump}=0.65.

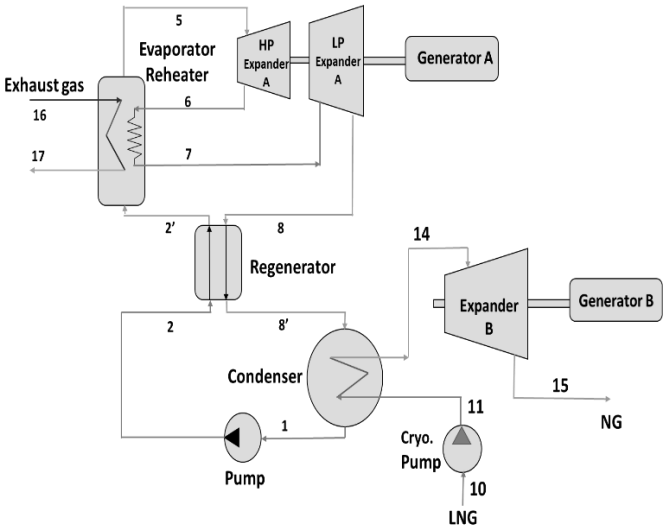

Fig. 5. Stage Regenerative Reheated ORC with Direct Expansion

The thermal efficiency of the system is:

$$\eta_{Thermal}=\frac{(\dot{W}_{5,6}+\dot{W}_{7,8}+\dot{W}_{14,15}-\dot{W}_{10,11}-\dot{W}_{1,2})\times\eta_{Evap.}}{\dot{Q}_{2'5}+\dot{Q}_{6,7}} \quad (31)$$

The exergy destruction on the 2 Stage ORC-DE system components is:

- Evaporator:

$$\dot{E}_{dEva.}=(\dot{E}_{x16}-\dot{E}_{x17})+(\dot{E}_{x2'}-\dot{E}_{x5})+(\dot{E}_{x6}-\dot{E}_{x7}) \quad (32)$$

- HP Expander:

$$\dot{E}_{dHPExpa.} = \dot{E}_{x5} - (\dot{E}_{x6} + \dot{W}_{5,6}) \quad (33)$$

- LP Expander:

$$\dot{E}_{dLPExpa.} = \dot{E}_{x7} - (\dot{E}_{x8} + \dot{W}_{7,8}) \quad (34)$$

- Regenerator:

$$\dot{E}_{dRegen.} = (\dot{E}_{x2} - \dot{E}_{x2'}) + (\dot{E}_{x8} - \dot{E}_{x8'}) \quad (35)$$

- Pump:

$$\dot{E}_{dPump} = \dot{E}_{x1} + \dot{W}_{1,2} - \dot{E}_{x2} \quad (36)$$

- Condenser:

$$\dot{E}_{dCon.} = (\dot{E}_{x8'} - \dot{E}_{x1}) + (\dot{E}_{x11} - \dot{E}_{x14}) \quad (37)$$

- Expander B:

$$\dot{E}_{dExpa.B} = \dot{E}_{x14} - (\dot{E}_{x15} + \dot{W}_{14,15}) \quad (38)$$

- Cryogenic Pump:

$$\dot{E}_{dCr.Pump} = \dot{E}_{x10} + \dot{W}_{10,11} - \dot{E}_{x11} \quad (39)$$

IV. Shell & Tube Heat Exchanger Modelling

The heat exchangers (Evaporator, Regenerator, and Condenser) for the ORC system are considered and modelled as counter-flow Shell and Tube (S&T) type HE. S&T HE are utilised mostly in the process industry as condensers in nuclear and conventional power stations and as exhaust gas generators in thermal, geothermal power plants [16]. Moreover, Single phase and two phase heat transfer (condensing, evaporating) can be utilized in either the tubes or the shell, in vertical or horizontal positions. The Pressure range and pressure drop are virtually unlimited. Thermal stresses can be sustained with low cost [17].

In heat exchanger operating above the dead state T0, both energy and exergy are transferred from hot stream to cold stream; whereas in heat exchanger operating below T0, energy is transferred from hot stream to cold stream, but exergy is transferred from cold stream to hot, Fig. 6 [18].

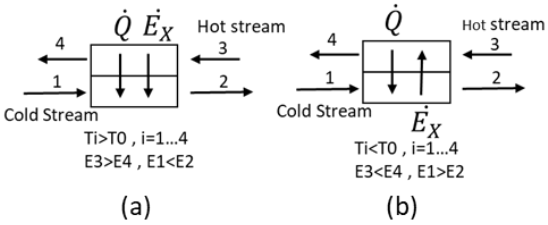

Fig. 6. Heat exchanger operating above 4(a) and below 4(b) dead state temperature (T_0)

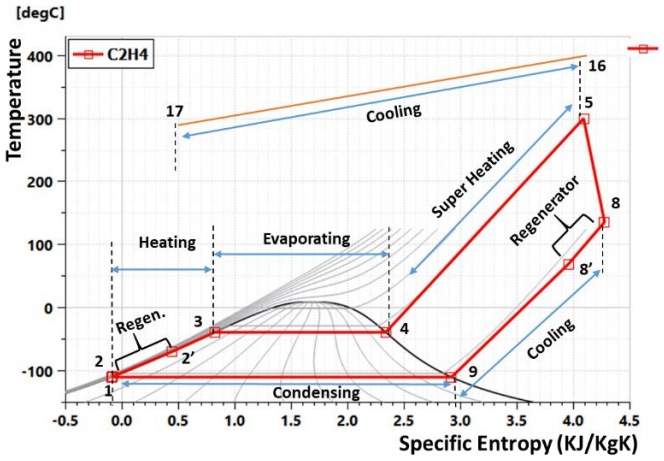

Fig. 7. Single stage ORC (WF C2H4) T-S diagram

As it is illustrated in Fig. 7, Fig. 8 HE are characterized in sections according to the state (liquid, wet vapour and vapour) of the fluids. Fig. 9 shows the division sections of Evaporator, Regenerator and Condenser. The Heating, Super-Heating, Cooling section express single flow heat transfer and the Evaporating/Boiling, Condensing section indicates two phase heat transfer.

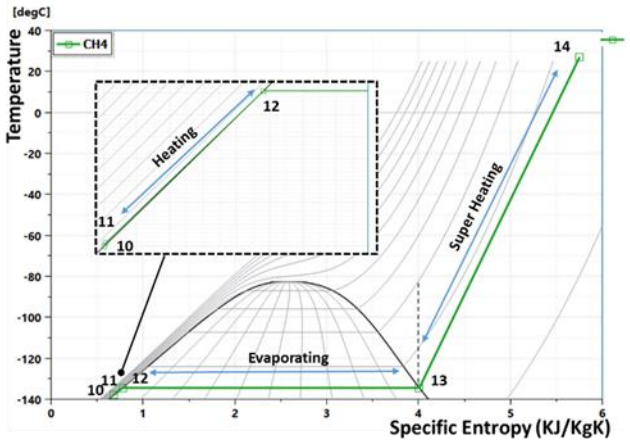

Fig. 8. LNG expansion process T-S diagram

For modelling HE the log-mean temperature difference (LMTD) for counter-flow arrangement method is used. According to Fig. 9 the evaporator is characterized by three sections: 1. tube-side heating & shell-side cooling, 2. tube-side evaporating & shell-side cooling, 3. tube-side superheating & shell-side cooling. For the tube-side heating & shell-side cooling section [19] the LMTD is,

$$LMTD_H = \frac{(T_A - T_3) - (T_{17} - T_{2'})}{\ln \frac{(T_A - T_3)}{(T_{17} - T_{2'})}} \quad (40)$$

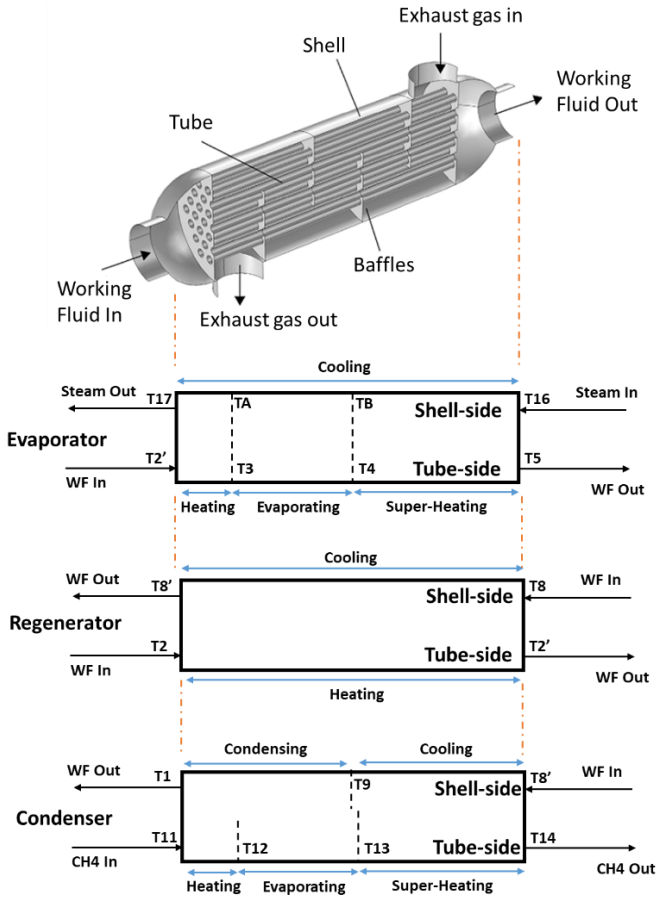

Fig. 9. Shell & Tube HE sections division

The corrected mean temperature difference is:

$$\Delta T_{m\_H}=F_C LMTD \tag{41}$$

The temperature correction factor (F_C=0.95) is defined by the correction factor graph [19] using the following parameters,

$$R=\frac{TA-T17}{T3-T2'} \tag{42}$$

$$S=\frac{T3-T2'}{TA-T2'} \tag{43}$$

A. Sizing of the Shell & Tube heat exchangers

The heat transfer area for the heating section between the hot and cold fluids is:

$$A_{Heating}=\frac{Q_{Heating}}{U_{Heating}\Delta T_{m\_H}} \tag{44}$$

Where,

$$Q_{Heating}= m_{WF}(T_3-T_{2'})\eta_{evap} \tag{45}$$

The heat transfer coefficient ($U_{Heating}$) is [16],

$$U_{Heating}= \left[\frac{1}{h_o}+R_{fo}+\frac{d_o \ln\frac{d_o}{d_i}}{2k_w}+\frac{d_o}{d_i}\frac{1}{h_i}+\frac{d_o}{d_i}R_{fi}\right]^{-1} \tag{46}$$

Where, h_o, h_i is the heat transfer coefficient of the shell and tube side for the heating section, respectively.

- d_i is the inner and d_0 is the outer diameter of tube,
- k_w is the wall material thermal conductivity,
- R_{fo} is the shell-side fluid fouling factor and R_{fi} is the tube-side fluid fouling factor.

Likewise the heat transfer area for the evaporating and super heating section are calculated. The overall heat transfer area for the evaporator HE is given as,

$$A_{total}=A_{Heating}+ A_{Evaporating}+A_{SuperHeating} \tag{47}$$

Similar procedure is followed for defining the total heat transfer area for Regenerator and Condenser.

TABLE III and TABLE IV present the Evaporator, Regenerator and Condenser design characteristics for Single and 2 Stage ORC arrangements, respectively, operating at 1.1bar condensing pressure.

TABLE III. : HE DESIGN CHARACTERISTICS FOR ORC - 1 STAGE C2H4 AT 1.1 PLOW

Evaporator			
Sections		**A**	**U**
Tube	**Shell**	**(m^2)**	**(W/m^2K)**
Heating	Cooling	0.0086	267.8
Evaporating	Cooling	5.8	255.8
Super Heating	Cooling	56.54	84.71
	Total	62.348	-
Regenerator			
Sections		**A**	**U**
Tube	**Shell**	**(m^2)**	**(W/m^2K)**
Heating	Cooling	86.45	14.85
	Total	86.45	-
Condenser			
Sections		**A**	**U**
Tube	**Shell**	**(m^2)**	**(W/m^2K)**
Super Heating	Cooling	10.55	243.39
Evaporating	Condensing	86.15	243.39
Heating	Condensing	2.69	137.56
	Total	99.39	-

With respect to TABLE III, for Single stage ORC the total heat transfer area of the heat exchangers is,

$$A_{Total}=62.348+86.45+99.39=248.18m^2$$

TABLE IV. HE DESIGN CHARACTERISTICS ORC - 2 STAGE C2H4 AT 1.1 P_{LOW}

Evaporator			
Sections		**A**	**U**
Tube	**Shell**	**(m^2)**	**(W/m^2K)**
Heating	Cooling	1.722	184.9
Evaporating	Cooling	9.570	158.2
Super	Cooling	93.19	74.78

Heating			
Reheating	Cooling	39.78	64.25
	Total	144.26	-
Regenerator			
Sections		**A**	**U**
Tube	**Shell**	**(m^2)**	**(W/m^2K)**
Heating	Cooling	37.07	15.08
	Total	37.07	-
Condenser			
Sections		**A**	**U**
Tube	**Shell**	**(m^2)**	**(W/m^2K)**
Super Heating	Cooling	25.21	98.1
Evaporating	Condensing	120.53	163.8
Heating	Condensing	31.03	127.96
	Total	176.77	-

The total heat transfer area of the heat exchangers for 2 stage ORC is,

$$A_{Total}=358.1m^2$$

Different correlation for calculating the heat transfer coefficients is used for single and two phase heat transfer, as it is analyzed in later paragraphs.

B. HE geometrical parameters

The selected geometrical parameters for the HE are assumed as: Fixed tube plate type, 1-shell and 1-tube pass exchanger (n_p=1) with 1″ OD tubes (14 BWG) on $1\frac{1}{4}''$ square pitch P_T and a pitch ratio of 1.25. OD is the tube outer diameter, d_o= 0.0254m. The tube fluid velocity is considered as u_t=2m/s to prevent erosion from high velocities and fouling from low velocities [16]. The tube material is stainless steel with thermal conductivity k_w=16W/mk. The baffle spacing is considered 40% of shell diameter and the baffle cut is set to 25%. The number of tubes (n_t=112) is taken corresponding to the closest standard shell ID of $17\frac{1}{4}''$ [19]. The fouling factor for the working fluids and methane is, R_F=0.00018 m^2K/W while the fouling factor for the exhaust gas is considered as R_F=0.00176 m^2K/W [20].

C. HE geometrical parameters

For tube side heating section, process (2, 2')-(2', 3)-(11, 12), and superheating process (4, 5)-(13, 14) single phase heat transfer and turbulent flow (Re>4000), the heat transfer coefficient (h_i) is calculated using the Petukhov-Kirillov correlation [16] as:

$$h_i=Nu\frac{k_t}{d_i} \tag{48}$$

Where Nu is the nusselt number which characterise the ratio of convective to conductive heat transfer. k is the thermal conductivity of the fluid and the tube inner diameter is di=0.02291m.

The Nusselt number is given as:

$$Nu=\frac{(f/2)\,RePr}{1.07+12.7(f/2)^{1/2}(Pr^{2/3}-1)} \tag{49}$$

Prandtl number is given as:

$$Pr=\frac{C_{pt}\mu_t}{k_t} \tag{50}$$

Where C_{pt} is the heat transfer coefficient, μ_t is the dynamic viscosity and k_t is the thermal conductivity of the tube side fluid.

Reynolds number is:

$$Re=\frac{u_t\rho_t d_i}{\mu_t} \tag{51}$$

The Filonenko's friction factor is calculated as:

$$f=(1.58\ln Re-3.28)^{-2} \tag{52}$$

D. Tube-side evaporating section

For tube side evaporating section, process (3, 4)-(12, 13), the heat transfer coefficient for boiling two phase heat transfer is calculated using the Chen and Shah's methods [16].

$$h_{lgt}=F_o(h_{LO}) \tag{53}$$

Using Shan's method the effect of stratification is defined. If Froude number in liquid phase Fr_{LO}>0.04 then the effects of stratification are negligible (inertial forces are dominant compared with gravitational) and Chen's correlation can be used [21], [22].

Froude Number is,

$$Fr_{LO}=\frac{G^2}{\rho_l^2 g d_i} \tag{54}$$

The mass velocity of the fluid (G) is given as,

$$G=\frac{(\rho_l+\rho_g)}{2}u_t \tag{55}$$

g is the gravitational acceleration and ρ_l,ρ_g denotes the fluid density in saturated liquid and vapour phase, respectively.

The enhancement factor is [23],

$$F_o=F(1-x_v)^{0.8} \tag{56}$$

Chen's method at dryness fraction $x_v = 0.05$ uses the Martinelli Parameter (X_{tt}),

$$\frac{1}{X_{tt}}=\left(\frac{x_v}{(1-x_v)}\right)^{0.9}\left(\frac{\rho_l}{\rho_g}\right)^{0.5}\left(\frac{\mu_g}{\mu_l}\right)^{0.1} \tag{57}$$

The convective boiling enhancement factor F is given as,

$$F=2.35\left(0.213+\frac{1}{X_{tt}}\right)^{0.736} \tag{58}$$

The liquid heat transfer coefficient (h_{LO}) according to Dittus-Boelter correlation as recommended by Shah is,

$$h_{LO}=\frac{Nu_{LO}k_l}{d_i} \tag{59}$$

The Nusselt number at $x_l=0$ regarding Gnielinski's correlation is,

$$Nu_{LO}=\frac{(f/2)(Re_{LO}-1000)Pr_{LO}}{1+12.7(f/2)^{1/2}(Pr_{LO}^{2/3}-1)} \tag{60}$$

Where the Reynolds number for the liquid phase is,

$$Re_{LO}=\frac{Gd_i}{\mu_l} \tag{61}$$

Prandtl number in liquid phase is,

$$Pr_{LO}=\frac{C_{pl}\mu_l}{k_l} \tag{62}$$

E. Shell-side cooling section

For Shell side cooling section, process (8, 8')-(8', 9)-(16, 17) single phase heat transfer, the heat transfer coefficient (h_o) is calculated by Macadam's correlation [24],

$$ho=\frac{k}{D_e}0.36\left(\frac{D_eG_s}{\mu_s}\right)^{0.55}\left(\frac{C_p\mu}{k}\right)^{1/3}\left(\frac{\mu_s}{\mu_w}\right)^{0.14} \tag{63}$$

$$(2000<Re=\frac{G_sD_e}{\mu_s}<1000000) \tag{64}$$

The factor $\Phi_s=\frac{\mu_s}{\mu_w}$ is considered unity.

The equivalent diameter for shell side for square pitch is,

$$D_e=\frac{4\left(P_T^2-\frac{\pi}{4}d_o^2\right)}{\pi d_o} \tag{65}$$

The pitch size is, $P_T=1.25d_o$. The mass velocity of the fluid in shell side is,

$$G_s=\frac{m_s}{a_s} \tag{66}$$

Where, m_s is the shell side fluid mass flow rate. The shell side cross flow area (a_s) is,

$$a_s=\frac{CBD_s}{P_T} \tag{67}$$

C is the tube clearance, $C=P_T-d_o$, and B is the Baffle spacing, B=0.4*Ds. The inside diameter of shell Ds is considered as, Ds =Db+BDC. BDC is the Bundle Diameter Clearance obtained from BDC chart for fixed tube HE [16] (BDC=12mm for Evaporator HE). Ds defines the shell fluid velocity.

The bundle diameter is estimated as,

$$Db=d_o\left(\frac{n_t}{K_1}\right)^{1/N_1} \tag{68}$$

K_1, N_1 are constants depending on the square pitch and number of tube passes (K_1=0.215 and N_1=2.207).

F. Shell-side condensing section

For shell side condensing section, process (9, 1) two phase heat transfer, the heat transfer coefficient h_{lgc} is calculated using Nusselt with Kern correction correlation [16].

$$h_{lgc}=0.728\left[\frac{\rho_l^2h_{LG}k_l^3}{\mu_l\Delta T_wd_o}\right]^{1/4}\frac{1}{n_t^{1/6}} \tag{69}$$

Where, h_{LG} is the enthalpy of condensation and ΔT_w is the difference between the temperature at the surface of the fouling and the liquid saturation temperature,

$$\Delta T_w=T_w-T_l \tag{70}$$

Where,

$$T_w=T_l+0.5\Delta T_m \tag{71}$$

G. Pressure drop

The tube side frictional pressure drop (Δp_{Total}), neglecting nozzle loss, is characterized by the fluid pressure drop (Δp_t) and by the sudden expansions and contractions that the tube fluid experiences during a return (Δp_r) [16].

$$\Delta p_{Total}=\Delta p_t+\Delta p_r \tag{72}$$

$$\Delta p_t=4f\frac{Ln_p}{d_i}\rho_t\frac{u_t^2}{2} \tag{73}$$

$$\Delta p_r=4n_p\frac{\rho_tu_t^2}{2} \tag{74}$$

Where,

$$f=0.046Re^{-0.2} \tag{75}$$

$$L=\frac{A_{Total}}{d_o\pi n_t} \tag{76}$$

The shell side pressure drop is calculated as [16]:

$$\Delta p_s=\frac{fG_s^2(N_b+1)D_s}{2\rho_sD_e\Phi_s} \tag{77}$$

Where,

$$N_b=\frac{L}{B}-1 \tag{78}$$

$$f=e^{(0.576-0.19\ln Re_s)} \tag{79}$$

$$400<Re_s=\frac{G_s D_e}{\mu_s}\leq 1\times 10^6 \quad (80)$$

V. Performance Analysis of Single and 2 Stages ORC Systems

A. Single stage Regenerative ORC performance analysis

According to Fig. 4, Fig. 7 and Fig. 8 the high pressure of the system is 15 bar while the condensing pressure is 1.1 bar (WF Ethylene). The temperature range of the T-S diagram is between -102ºC and 300ºC. The ORC T-S cycle is heated up to 300ºC so as to be able to super heat the LNG up to 27ºC. Thus, point T8' > T14. The work output of the cycle is $W_{5,8}$ = 346.6KW. The thermodynamic properties of the working fluid, exhaust source and LNG source are presented in Table V and Table VI.

Table V. Thermodynamic properties of ORC TS states

No	T (ºC)	P (Bar)	h (KJ/Kg)	s (KJ/KgK)	$\dot{m}$ (Kg/s)	$\dot{E}x$ (KW)
1	-102.4	1.1	3.396	0.0198	1.133	432.8
2	-101.4	15	7.172	0.0275	1.133	434.6
2'	-39.1	15	167.17	0.8185	1.133	357.7
5	300	15	1204.7	4.0889	1.133	466.2
8	158.2	1.1	894.92	4.2417	1.133	65.07
8'	52.60	1.1	702.93	3.7337	1.133	13.26
10	-138	5	84.760	0.6802	0.875	790.3
11	-137.7	6	85.159	0.6812	0.875	790.4
14	27	6	909.17	5.7535	0.875	233.2
16	400	1.3	-	-	10.44	1714
17	284.2	1.3	-	-	10.44	965.1

Table VI. Thermodynamic properties of ORC TS states

No	Cp (J/KgK)	μ × (10^{-5}) (Kg/ms)	k (W/mK)	ρ (Kg/m^3)
1	2406.9	17.227	0.18515	565.914
2	2399.3	17.005	0.18544	565.967
2'	2925.2	8.0887	0.12160	459.219
5	2466.7	1.8800	0.06330	8.8889
8	2002.2	1.4548	0.03940	0.86191
8'	1631.3	1.1242	0.02396	1.14477
10	3731.5	7.2760	0.15077	385.727
11	3729.6	7.2764	0.15080	385.746
14	2264.8	1.1282	0.03472	3.89673
16	1182.3	3.096	0.04880	0.66467
17	1145.4	2.680	0.04121	0.80325

Table VII. Exergy destruction and exergy destruction ratios

Component	$\dot{E}_d$ (KW)	E_{DR}
Evaporator	640.26	0.4903
Expander	49.893	0.0382
Regenerator	128.68	0.0985
Condenser	137.62	0.1054
Pump	2.514	0.0019
Cryo. Pump	0.252	0.0002

The thermal efficiency of the system is:

$$\eta_{Thermal}=23.58\%$$

The second law efficiency is:

$$\eta_{Ex}=24.55\%$$

The percentage of exergy destruction in each component of the ORC system is depicted in Fig. 10. The evaporator is the component of the ORC system demonstrating the highest percentage (67%) of exergy destruction and the lowest exergetic efficiency of 14.49%. The regenerator and condenser is characterized by a 14% of exergy destruction with relatively high exergetic efficiency of 67.37% and 75.3%, respectively. Both pumps presents negligible exergy destruction whilst the expander demonstrates the highest exergetic efficiency (87.56%).

$$\eta_{ExEvap}=1-\frac{\dot{E}_{dEva}}{\dot{E}_{x16}-\dot{E}_{x17}}\times 100\%=14.49\% \quad (81)$$

$$\eta_{ExCon.}=1-\frac{\dot{E}_{dCon.}}{\dot{E}_{x11}-\dot{E}_{x14}}\times 100\%=75.3\% \quad (82)$$

$$\eta_{ExReg.}=\frac{\dot{E}_{x8}-\dot{E}_{x8'}}{\dot{E}_{x2}-\dot{E}_{x2'}}\times 100\%=67.37\% \quad (83)$$

$$\eta_{ExPump.}=1-\frac{\dot{E}_{dpump}}{\dot{W}_{pump}}\times 100\%=41.2\% \quad (84)$$

$$\eta_{ExPCryopump.}=1-\frac{\dot{E}_{dCryopump}}{\dot{W}_{pump}}\times 100\%=27.81\% \quad (85)$$

$$\eta_{ExExpan.}=1-\frac{\dot{E}_{dExpander}}{\dot{E}_{x5}-\dot{E}_{x8}}\times 100\%=87.56\% \quad (86)$$

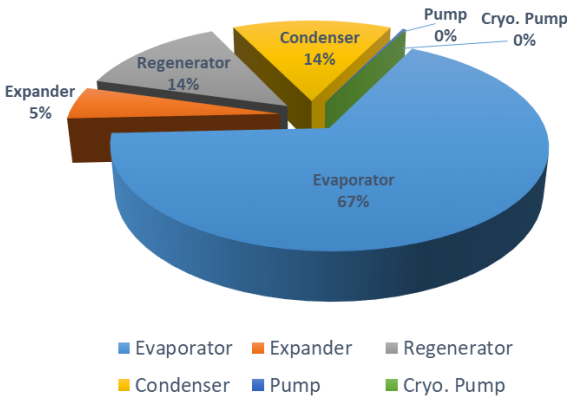

Fig. 10. Exergy destruction percentage (E_D(%)) in each component of the single stage ORC system

In Fig. 11, between 1.1 and 2.5 bar condensing pressure the exergy destruction ratio on the evaporator is reduced by 2.15%, whilst on the condenser is increased by 14.25%. According to Equation 16 the cumulative exergy destruction ratios with the exergy efficiency is proportional to unity,

$$\eta_{Ex}+E_{DREva}+E_{DRExpan}+E_{DRRegene}+E_{DRCond}+E_{DRPump}$$

$$+E_{DRCryoPump}=1 \quad (87)$$

Thus, the reduction of exergy efficiency in higher condensing pressures is affected mostly by the increased exergy destruction on the condenser of the ORC system.

In Fig. 12 is depicted the thermal efficiency of the ORC system operating with Ethylene, Butane and Propane from 0.01 to 2.5 bar condensing pressure (P_{Low}). For high vacuum pressures (P_{Low} =0.01bar) the system demonstrates the higher thermal efficiency (32.59%) with WF R290. At low vacuum pressure (P_{Low} =0.5bar) WF C2H4 shows the higher thermal efficiency (28.44%). For C2H4 at P_{Low} =0.5bar in liquid phase (x=0), the saturated liquid temperature is, T=-115ºC, which is the lower limit boundary selected for the thermodynamic cycle; thus, high vacuum pressures (below 0.5bar) for C2H4 are not considered for further analysis. R290 presents the higher thermal efficiency reduction (by 19.74%) from high vacuum up to 2.5bar.

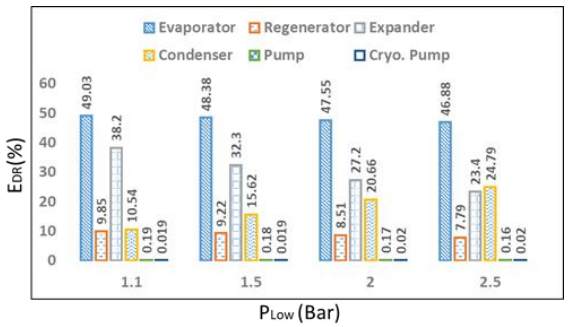

Fig. 11. Exergy destruction percentage ratios (E_{DR}(%)) in each component of the single stage ORC system for C2H4

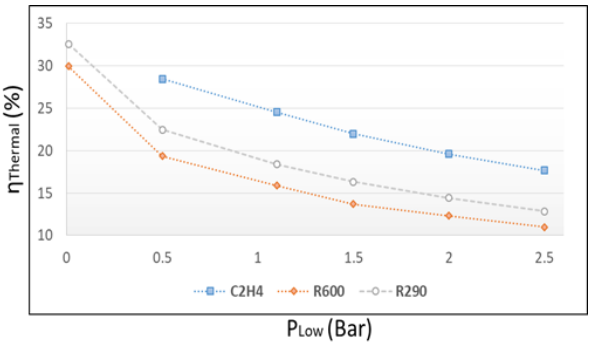

Fig. 12. ORC thermal efficiency fluctuation for WF C2H4, R600, R290 for PLOW 0-2.5bar

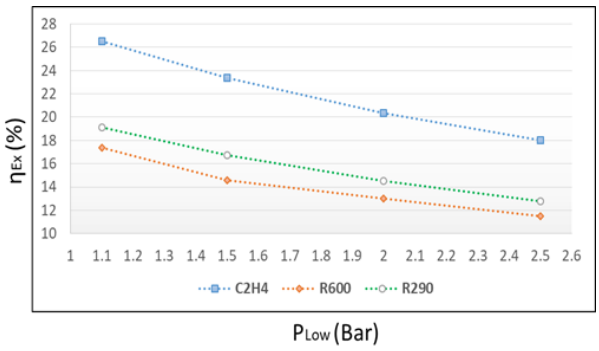

Fig. 13. ORC exergy efficiency fluctuation for WF C2H4, R600, R290 for PLOW 1.1-2.5bar

Fig. 13 shows the exergy efficiency of the ORC system. C2H4 demonstrates the highest η_{EX} = 26.54% at P_{LOW}=1.1bar, 9.18% and 7.43% higher than R600 and R290, respectively. In Fig. 14, the ORC system operating in high vacuum with WF R290 demonstrates work output of 528.8KW while with WF R600 the work output is slightly reduced to 508KW. However, when the condensing pressure increases at 0.5bar, C2H4 presents the highest work output of 428.8KW.

With WF R600 from high vacuum up to 0.5bar condensing pressure the ORC work production is reduced by 44%. Thus, the utilization of high vacuum pressures increases the work produced by the ORC significantly. But, the construction of a condenser operating in vacuum pressure increases the complexity and cost of the system. In particular in vacuum pressure the ORC is characterized by a condenser with large surface area, a complex turbine and air leakage concerns [25].

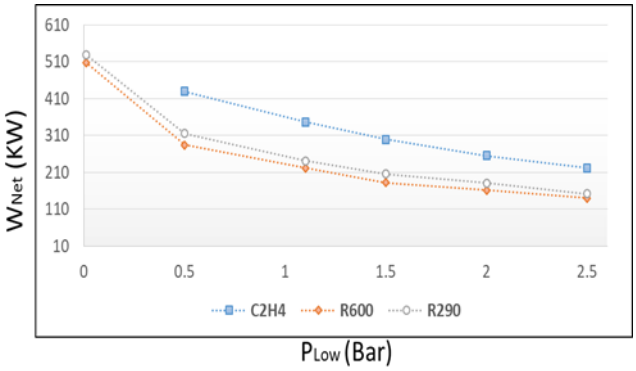

Fig. 14. ORC work output fluctuation for WF C2H4, R600, R290 for PLOW 0.01-2.5bar

B. *Two stage Regenerative Reheated ORC with Direct Expansion performance analysis*

Fig. 15, shows the Temperature-Entropy (T-S) diagram of the 2 stage ORC cycle (Fig. 5), while Fig. 16 illustrates the T-S diagram of the LNG direct expansion cycle.

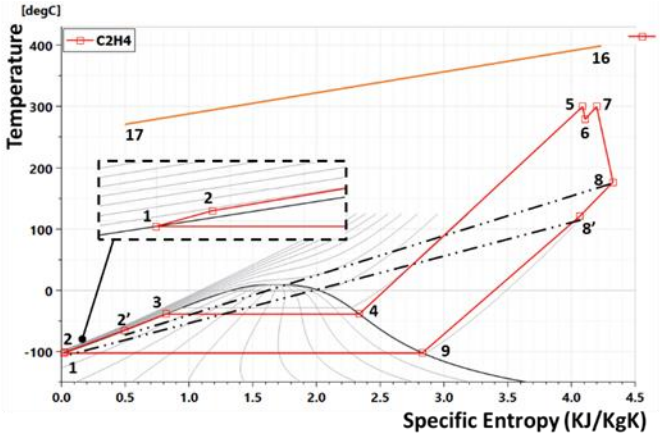

Fig. 15. Two stage Reheated ORC (WF C2H4) T-S diagram

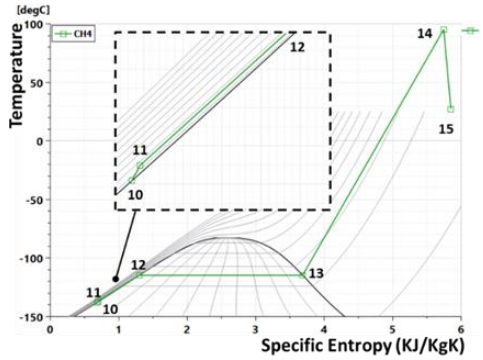

Fig. 16. LNG direct expansion cycle T-S diagram

TABLE VIII & TABLE IX present the thermodynamic properties in each state (1-17) of the two stage ORC at 1.1bar condensing pressure.

TABLE VIII. THERMODYNAMIC PROPERTIES OF ORC TS STATES

No	T (ºC)	P (Bar)	h (KJ/Kg)	s (KJ/KgK)	$\dot{m}$ (Kg/s)	$\dot{E}x$ (KW)
1	-102.4	1.1	3.396	0.0198	1.173	447.7
2	-101.4	15	7.172	0.0275	1.173	449.6
2’	-59.43	15	111.17	0.56847	1.173	388.8
5	300	15	1204.7	4.0889	1.173	482.3
6	279.04	10.5	1155.8	4.1071	1.173	418.8
7	300	10.5	1206.7	4.1976	1.173	448.0
8	176.63	1.1	932.30	4.3266	1.173	65.07
8’	109.97	1.1	802.30	4.0142	1.173	35.52
10	-138	5	84.760	0.6802	0.875	790.3
11	-137.2	15	88.744	0.6905	0.875	791.2
14	95	15	1062.8	5.7446	0.875	369.9
15	27	5	910.36	5.8511	0.875	209.6
16	400	1.3	-	-	10.44	1714
17	267.8	1.3	-	-	10.44	869.8

TABLE IX. THERMODYNAMIC PROPERTIES OF ORC TS STATES

No	Cp (J/KgK)	$\mu \times (10^{-5})$ (Kg/ms)	k (W/mK)	ρ (Kg/m^3)
1	2406.9	17.227	0.18515	565.914
2	2399.3	17.005	0.18544	565.967
2’	2616.6	10.351	0.14157	500.026
5	2466.7	1.8800	0.06330	8.8889
6	2401.1	1.8147	0.05915	6.4534
7	2459.4	1.8705	0.06317	6.2104
8	2064.4	1.5088	0.04217	0.82647
8’	1833.8	1.3083	0.03220	0.97146
10	3731.5	7.2760	0.15077	385.727
11	3713.1	7.2797	0.15111	385.920
14	2475.9	1.3507	0.04540	7.94583
15	2259.1	1.1268	0.03467	3.24067
16	1182.3	3.096	0.04880	0.66467
17	1140.4	2.619	0.04013	0.82735

Table x, depicts the exergy destruction in each component of the two stage ORC system. The evaporator is characterized by significant high exergy destruction of around 721KW while the condenser exergy destruction is negligible.

TABLE X. EXERGY DESTRUCTION IN EACH COMPONENT

Component	E_d (KW)
Evaporator	721.39
HP Expander	6.14
LP Expander	43.57
Regenerator	107.68
Condenser	9.025
Pump	2.60
Expander B	26.84
Cryo. Pump	2.59

The thermal efficiency of the system is:

$$\eta_{Thermal}=31.34\%$$

The second law efficiency is:

$$\eta_{Ex}=35.43\%$$

Fig. 17 depicts the exergy destruction percentage (Ed(%)) and the exergy efficiency (Equations 81-86) for each component of the system operating with WF C2H4 at P_{Low}=1.1bar. The evaporator shows the highest exergy destruction percentage of 78%, while the exergy destruction in the condenser is 1%. All the heat exchangers of the system counts for 91% of the total exergy destruction.

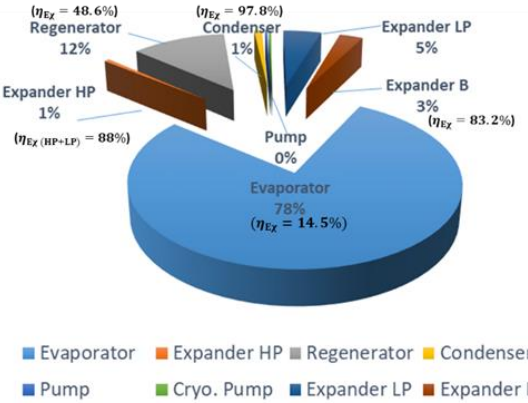

Fig. 17. Exergy destruction percentage (E_D(%)) in each component of the two stage ORC system

Fig. 18 presents the exergy destruction ratios percentage for two stage ORC-DE with WF C2H4 between 1.1 to 2.5bar condensing pressure. The increased E_{DR} (%) of the condenser and regenerator results to the exergy efficiency reduction of the ORC system. Specifically, the condenser E_{DR} (%) becomes greater by 10.51% while the regenerator E_{DR} (%) increases only by 0.71%. Therefore, the condenser E_{DR} (%) increment affects negatively the ORC exergy efficiency.

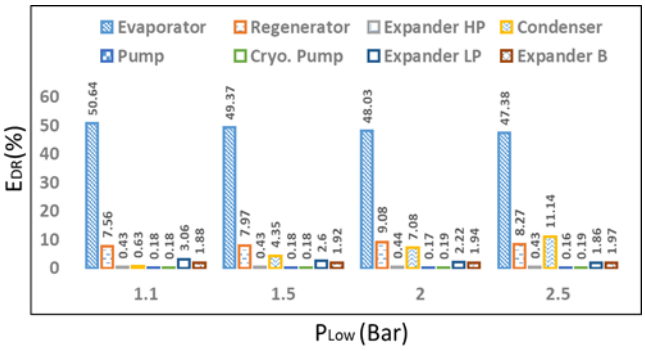

Fig. 18. Exergy destruction percentage ratios (EDR(%)) in each component of the two stage ORC system

Fig. 19 presents the fluctuation of C2H4, R290 and R600 Thermal efficiency for condensing pressure between 0.01bar and 2.5bar. R290 shows the highest thermal efficiency of 35.66% at high vacuum pressure. However, from low vacuum pressure up to 2.5bar C2H4 is linearly more thermal efficient by 6.35% and 9.28% than R290 and R600, respectively.

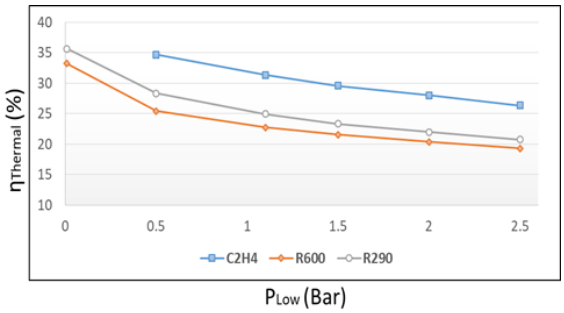

Fig. 19. Two stage ORC thermal efficiency fluctuation for WF C2H4, R600, R290 for PLOW 0-2.5bar

In Fig. 20, for the condensing pressure range between 1.1 - 2.5bars C2H4 demonstrates also linear higher exergy efficiency difference by 7.54% and 10.41% compared to R290 and R600, respectively.

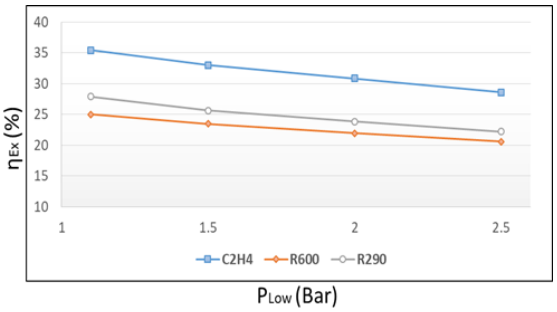

Fig. 20. Two stage ORC exergy efficiency fluctuation for WF C2H4, R600, R290 for PLOW 1.1-2.5bar

In Fig. 21, the network of the system in high vacuum pressure in significantly increased for R290 up to 650KW while for R600 is 591.7KW. But, from 0.5-2.5bars P_{Low}, C2H4 presents the highest Net-work of 587.27KW to 388.63KW. C2H4 at P_{LOW}=0.5bar compared to R290 at P_{Low}=0.01bar indicates W_{Net} reduced only by 10%. Therefore, Ethylene at low vacuum pressure shows similar performance like R290 and R600 operating in high vacuum pressure.

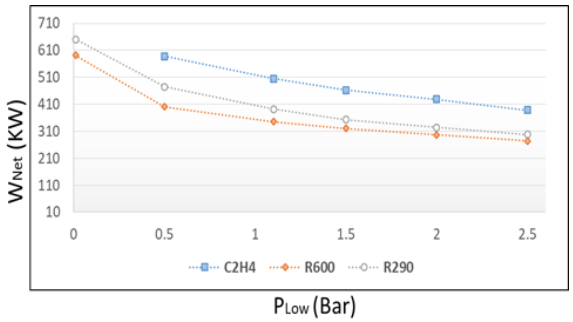

Fig. 21. ORC work net fluctuation for WF C2H4, R600, R290 for PLOW 0-2.5bar

VI. Economic Analysis of the Proposed ORC Systems

The proposed ORC power plants are economically evaluated with respect to the specific investment cost (SIC) of the power plant [26] in $/KW.

$$SIC=\frac{C_{TM}\times OMC}{W_{Net}} \tag{88}$$

The operating and maintenance cost (OMC) is considered as 2% [27] of the total capital cost. W_{Net} is the net work output of the power plant.

The total capital cost (total module) of the ORC power plant (C_{TM}) is defined as the sum of the capital cost of the individual equipment.

$$C_{TM}=\frac{CEPSI\ 2016}{CEPSI\ 2001}F_s\sum_{i=1}^{n}C_{BM,i} \tag{89}$$

For accounting inflation the Chemical Engineering Plant Cost Index (CEPSI) ratio is used (CEPSI 2016=541.7, CEPSI 2001=397 [28]). The additional factor (F_s) for the overhead cost is considered unity.

The capital recovery factor (CRF) is,

$$CRF=\frac{i(1+i)^{n_{pl}}}{(1+i)^{n_{pl}}-1} \tag{90}$$

Where, i is the interest rate and n_{pl} is the ORC power plant expected life cycle [29] (i=5%, n_{pl}=20years).

The levelized electricity cost (LEC) is the cost of generating electricity for the ORC [30].

$$LEC=\frac{CRF\times C_{TM}+OMC}{W_{Net}\times h_{full\text{-}load}} \tag{91}$$

Where, $h_{full\text{-}load}$ is the full load annual operation hours, ($h_{full\text{-}load}$=8000hr/a).

A. *Heat Exchangers*

The bare module cost for S&T HE fixed tube sheet is given as [31],

$$C_{BM,1}=C_{p1}^{0}F_{BM}=C_{p1}^{0}[B_1+B_2F_{P1}F_{M1}] \tag{92}$$

Where,

F_{BM} is the bare module cost factor,

B_1=1.63, B_2=1.66

The pressure factor is,

$$\log_{10}F_{P1}=C_1+C_2\log_{10}P+C_3(\log_{10}P)^2 \tag{93}$$

P is the barg or bar gauge pressure ($P=P_{abs}$-1).

For P<5barg,

$$C_1=C_2=C_3=0$$

For 5<P<140barg,

$$C_1=0.03881,\ C_2=-0.11272,\ C_3=0.08183$$

The material factor is, $F_{M1}=2.7$ for stainless steel Shell and tube side HE.

The purchased cost of the equipment is given as,

$$\log_{10}C_{p1}^0=K_1+K_2\log_{10}(A)+K_3[\log_{10}(A)]^2 \quad (94)$$

Where, A (m^2) is the total heat transfer area of the HE.

For fixed tube,

$$K_1=4.3247,\ K_2=-0.3030,\ K_3=0.1634$$

B. Expander

The Expanders are considered as carbon steel with axial arrangement. The bare module cost is [31],

$$C_{BM,2}=C_{p2}^0F_{M2} \quad (95)$$

Where,

$$C_{p2}^0=K_1+K_2\log_{10}(Wout)+K_3[\log_{10}(Wout)]^2 \quad (96)$$

Wout (KW) is the work output of the expander, the constants for the expander type are,

$$K_1=2.7051,\ K_2=1.4398,\ K_3=-0.1776$$

Valid for the range, 100(KW)<Wout<4000(KW)

The material factor for carbon steel is, $F_{M2}=3.5$.

C. ORC Pump

Both pumps are assumed to be centrifugal made of stainless steel.

The bare module cost is [31],

$$C_{BM,3}=C_{p3}^0[B_1+B_2F_{P3}F_{M3}] \quad (97)$$

$$(B_1=1.89,\ B_2=1.35)$$

The pressure factor is,

$$\log_{10}F_{P3}=C_1+C_2\log_{10}(P)+C_3\left(\log_{10}P\right)^2 \quad (98)$$

For, 10<P<100barg,

$$C_1=-0.3935,\ C_2=0.3957,\ C_3=-0.00226$$

The purchased cost of the equipment is,

$$\log_{10}C_{p3}^0=K_1+K_2\log_{10}(Win)+K_3[\log_{10}(Win)]^2 \quad (99)$$

Win is the shaft work input to the pump.

For, 1(KW)<Win<300(KW)

$$K_1=3.3892,\ K_2=0.0536,\ K_3=0.1538$$

The material factor is, $F_{M3}=2.3$.

D. Cryogenic Pump

For operating pressure P<10barg the bare module cost is [31],

$$C_{BM,4}=C_{p4}^0F_{M4} \quad (100)$$

The purchased cost of the equipment is,

$$\log_{10}C_{p4}^0=K_1+K_2\log_{10}(Win)+K_3\left[\log_{10}(Win)\right]^2 \quad (101)$$

The constants for the pump type are,

$$K_1=3.3892,\ K_2=0.0536,\ K_3=0.1538$$

The material factor for stainless steel is, $F_{M4}=2.3$.

E. Turbine Size

The turbine size parameter is defined as,

$$SP=\frac{\dot{V}_{out}^{0.5}}{\Delta h^{0.25}\times 10^3} \quad (102)$$

Where, $\dot{V}_{out}$ is the expander output volumetric flow rate and Δh is the enthalpy difference of the WF between input and exit of the expander [32].

The expander volumetric expansion ratio between the outlet and inlet volumetric flow rate is given as,

$$V_r=\frac{\dot{V}_{out}}{\dot{V}_{in}} \quad (103)$$

VII. Comparison in Thermodynamic & Economic Characteristics of Single Stage and Two Stage ORC Arrangements

In this chapter the Energetic analysis is demonstrated from high vacuum up to 2.5bar condensing pressure; whereas the exergetic and economic analysis is considered only for the most efficient WF between 1.1bar to 2.5bar condensing pressure.

TABLE XI presents the most thermal efficient WF among high, low vacuum and 2.5bar condensing pressure between single and two stage ORC. At high vacuum pressure R290 presents a thermal efficiency of 32.6% while in two stage ORC R290 demonstrates thermal efficiency of 35.66%; 2 stage ORC produces 18.64% higher work output.

At low vacuum pressure (P_{Low}=0.5bar) Ehtylene is the most promising WF with thermal efficiency of 28.44% for single

stage ORC and improved by 7.22% up to 34.7% for two stage ORC; the respective work output for the two stage ORC is increased by 27%. At 2.5bar condensing pressure two stage ORC shows 43% higher work output and is more thermal efficient by 8.68% than single stage ORC with WF C2H4. Overall, the 2 Stage ORC demonstrates significant increment in thermal efficiency and work output than single stage (especially in higher values of condensing pressure).

TABLE XI. ENERGY COMPARISON BETWEEN SINGLE AND TWO STAGE ORC

Single stage ORC		
P_{LOW} = 0.01bar		
	$\eta_{Thermal}$ (%)	W_{Net} (KW)
R290	32.6	528.8
P_{LOW} = 0.5bar		
	$\eta_{Thermal}$ (%)	W_{Net} (KW)
C2H4	28.44	428.8
P_{LOW} = 2.5bar		
C2H4	17.66	221.5
Two stages ORC		
P_{LOW} = 0.01bar		
	$\eta_{Thermal}$ (%)	W_{Net} (KW)
R290	35.66	650
P_{LOW} = 0.5bar		
	$\eta_{Thermal}$ (%)	W_{Net} (KW))
C2H4	34.7	587.27
P_{LOW} = 2.5bar		
C2H4	26.34	388.6

According to Fig. 13 and Fig. 20 the most exergetic efficient WF at condensing pressure between 1.1 to 2.5bar is C2H4; 2 Stage ORC shows 10% higher exergy efficiency than single Stage for the entire condensing pressure range.

As far as the exergy destruction in each component is concerned, regarding Fig. 10 and Fig. 17, single stage ORC illustrates 14% and 67% exergy destruction in the condenser and evaporator, respectively. However, two stage ORC presents negligible exergy destruction in the condenser and 11% less in the evaporator. For both arrangements the exergy destruction percentage in heat exchangers is around 95%. Also, the exergy destruction fluctuation in the condenser affects the exergy efficiency in each ORC system.

Fig. 22 illustrates the estimation in the sustainability of the systems using the Sustainability Index approximation. Two stage ORC operating with C2H4 - 2 Stage is the most sustainable system and presents the highest sustainability at 1.1bar condensing pressure; compared to C2H4 – 1 Stage shows 12.1% higher Sustainability Index. Also, C2H4 - 1 Stage presents almost the same SI with R600 - 2 Stage.

The expander Size Parameter (Equation 102) and the volumetric expansion ratio (Equation 103) is,

$$SP=0.0486m,\ V_r=10.34\ ,$$

The total capital cost (equation) of the ORC system is,

$$C_{TM}=1.39\times10^6\$$$

The specific investment cost (equation) is,

$$SIC=4092\$/KW$$

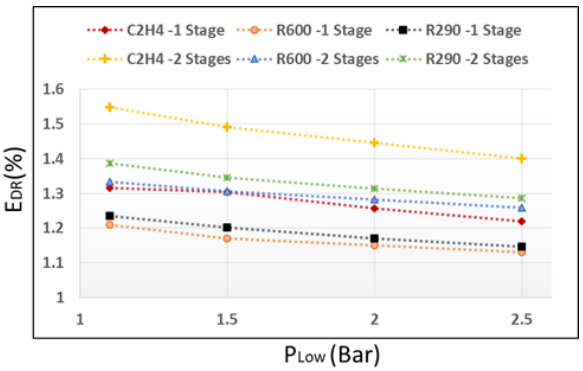

Fig. 22. Sustainability Index of ORC systems

The levelized electricity cost (equation) is,

$$LEC=0.0402\$/KWh$$

TABLE XII. DESIGN & ECONOMIC CHARACTERISTICS FOR ORC 1-STAGE AT $1.1P_{Low}$ OPERATING WITH C2H4

P_{LOW} (Bar)	A_{Total} (m^2)	SP (m)	V_r	C_{TM} $\times 10^6$ ($)	SIC $/KW	LEC $/KWh
1.5	230	0.049	10.3	1.315	4490	0.044
2	147	0.044	7.8	1.185	4742	0.046
2.5	92.7	0.034	4.9	1.088	5010	0.049

According to TABLE XII the decrease in condensing pressure results to higher heat transfer area of the heat exchangers and to higher volumetric ratio and size parameter for the expanders. Consequently, the larger design values for the ORC components lead to higher total capital cost (C_{TM}). However, al low condensing pressure the produced Net-work is higher (Fig. 14); thus, the specific investment cost and the levelized electricity cost is lower. TABLE XIII presents the Design and Economic characteristics for ORC 2-Stage operating with WF C2H4 at 1.1bar condensing pressure.

TABLE XIII. DESIGN & ECONOMIC CHARACTERISTICS FOR ORC 2-STAGE AT 1.1PLOW OPERATING WITH C2H4

P_{LOW} (Bar)	A_{Total} (m^2)	SP_{Total} (m)	$V_{r_{Tot.}}$	C_{TM} $\times 10^6$ ($)	SIC $/KW	LEC $/KWh
1.1	358	0.107	11.3	2.093	4309	0.042
1.5	344	0.101	9.5	2.038	4497	0.044
2	360	0.097	8.2	1.997	4761	0.047
2.5	478	0.093	7.4	2.061	4913	0.048

The total expander size parameter ($SP_{Total}=SP_{HP}+SP_{LP}+SP_B$) and volumetric ratio is given as the sum of the HP, LP and B expander.

According to TABLE XIII in 2-Stage ORC the total heat transfer area of the heat exchangers is increased from 30% up to 80% compared to 1-Stage ORC due to the Evaporator Reheating process and to vaporization of the LNG at 15bars. The total expander size parameter for 2-Stage ORC is almost double that the 1-Stage ORC since the addition of 2 expanders.

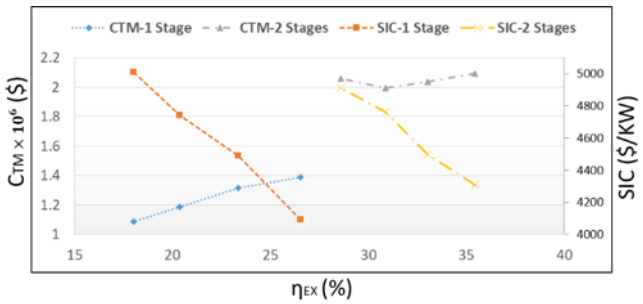

Fig. 23. Capital cost and specific investment cost with respect to exergy efficiency of ORC systems

Fig. 23 depicts the fluctuation of the total capital cost and the specific investment cost for both ORC arrangements with respect to the system exergy efficiency. The total capital cost for the 2-Stage ORC remains almost constant at $2 million dollars and is 60% up to 90% higher than the C_{TM} of the 1-Stage ORC. However, the 2-Stage ORC demonstrates higher exergy efficiency of 10% for the same expander pressure ratio and relatively small difference (around 2%) in specific investment cost.

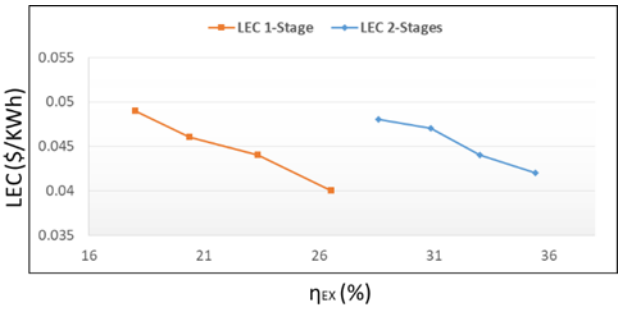

Fig. 24. Levelized electricity cost with respect to exergy efficiency of ORC systems

In accordance to Fig. 24 the levelized electricity cost between 2-Stage ORC and 1-Stage ORC differs by almost 5%. Above 1.1 condensing pressure the 2-Stage ORC presents better economic performance and is one third more exergetic efficient than 1-Stage ORC.

VIII. Scenario Analysis of the Fuel Consumption Saving & the ORC System Payback Time

The fuel consumption saving on a LNG powered case vessel is considered while the ORC is operating above atmospheric condensing pressure with WF C2H4. Specifically, the fuel consumption (FC) in NG at the optimum speed is 0.875Kg/s producing 20MW of Power (P_{Ferry}).

For 1-Stage ORC and P_{Low}=1.1bar the work output (W_{Net}) is 346.6 KW saving 1.733% of NG or the fuel consumption saving in NG is,

$$FCS_{NG}=\frac{FC \times W_{Net}}{P_{Ferry}} \times 3600 = 54.589 Kg/h$$

Considering the following parameters:

- 8000 operation hours annually (h/a)
- 1 ton of NG = 68.79mmbtu (NG_{mmbtu})
- 1ton of LNG = 52mmbtu (LNG_{mmbtu})
- LNG cost = 11.46$/mmbtu ($LNG_{cost}$)

The LNG_{cost} is a very sensitive parameter and is considered as the average LNG cost ($/mmbtu) between 2007-2017 given for LNG Japan import price [33].

Using the mmbtu conversion, the NG consumption saving per year is 436.712ton/year or for LNG consumption saving/year is,

$$FCS_{LNG}=\frac{FCS_{NG} \times h/a \times NG_{mmbtu}}{LNG_{mmbtu}} \times 10^{-3} =>$$

$$FCS_{LNG}=577.72 \text{ LNG ton/year}$$

The fuel consumption cost saving (FCCS) per year is,

$$FCCS=FCS_{LNG} \times LNG_{mmbtu} \times LNG_{cost} =>$$

$$FCCS=344{,}285\$/year$$

The payback time (PT) is assumed as,

$$PT=\frac{C_{TM}}{FCCS}=4 \text{ years}$$

Fig. 25 presents for both ORC arrangements the Fuel consumption cost saving per year and the Payback time with respect to Low Pressure range between 1.1 and 2.5bar.

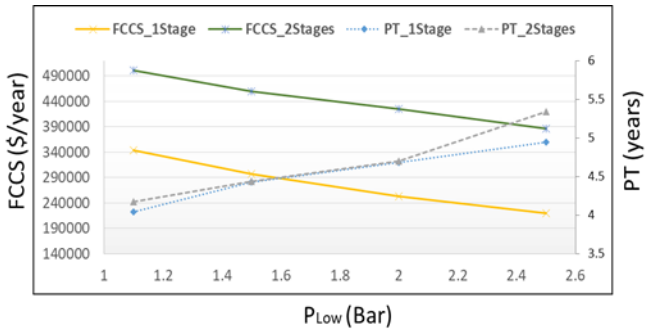

Fig. 25. Fuel cost saving/year and Payback time with respect to exergy efficiency of ORC systems

At 1.1bar 1 & 2-Stages ORC presents the highest FCCS/year and the lowest payback time at around 4 years. Although 2-Stage ORC demonstrates 31% higher FCCS/year than 1-Stage for the entire condensing pressure range, the payback time is almost the same up to 2bar fluctuating from 4 to 4.7 years.

IX. Conclusions

The current vessel's LNG cold energy recovery system demonstrates 55% losses of LNG cold energy. The LNG cold energy between -138°C to 133°C (including the enthalpy of formation) is dissipated through pipes and only a part of the sensible heat is utilized. The proposed dual utilization of thermal

waste and LNG cold energy is examined with single and two stage ORC with constant evaporating pressure at 15bars.

In both arrangements above 0.5 bars condensing pressure the most efficient WF is Ethylene. In 1-Stage ORC at 0.5bar low pressure, C2H4 presents 28.44% thermal efficiency with work output of 428.8KW; for the respective vacuum pressure 2-Stage ORC with WF C2H4 shows 34.7% thermal efficiency and 587.27KW work output. However, at high vacuum pressure (0.01bar) 2-Stage ORC WF Propane demonstrates 650KW work output and a thermal efficiency of 35.66%. Above vacuum the most efficient condensing pressure is at 1.1bar; in which single Stage ORC WF C2H4 is characterized by a 23.58% thermal and 24.55% exergy efficiency while 2-Stage ORC illustrates more than one-third improvement in thermal and exergy efficiency.

1-Stage ORC shows 67% exergy destruction in the evaporator and 14% in the condenser; whereas, 2-Stage ORC demonstrates 78% exergy destruction in evaporator and negligible in the condenser. In both arrangements the higher exergy destruction occurs in the evaporator and condenser. Specifically, 95% of the total exergy destruction taking place in the heat exchangers of the ORC systems. The increase in exergy destruction on the condenser contributes to the decrease of the exergy efficiency of the system.

At 1.1bar condensing pressure the heat transfer area of the ORC heat exchangers, the expander size parameter and the volumetric ratio is the highest, resulting to higher total capital cost. However, the increased ORC work output at 1.1bar leads to a lower specific investment cost. For 1-Stage ORC at 1.1bar is 4092$/KW while for 2-Stage ORC the SIC is 4309$/KW. The fuel consumption saving per year for 1-Stage ORC is 344,285$/year with a payback time of 4 years; 2-Stage ORC presents 31% improved FCCS/year with almost 4years PT. Overall, at 1.1bar condensing pressure 2-Stage ORC shows better thermodynamic and economic performance by one-third compared to single Stage ORC saving around 2.5% of Ferry's NG consumption.

ACKNOWLEDGMENT

This study was funded through the project of the EPSRC Prosperity Outcomes Award. The fund was allocated to Newcastle University by the UK Engineering and Physical Sciences Research Council (EPSRC). The authors appreciate all the support received from both Newcastle University and the EPSRC.

REFERENCES

[1] IMO (2016), Available at : http://www.imo.org/en/OurWork/environment/pollutionprevention/airpollution/pages/air-pollution.aspx

[2] Yuksek, E. and Mirmobin, P. (2015) WASTE HEAT UTILIZATION OF MAIN PROPULSION ENGINE JACKET WATER IN MARINE APPLICATION. Brussels.

[3] Ahlgren, F., Mondejar, M., Genrup, M., and Thern, M. (2015) Waste Heat Recovery in a Cruise Vessel in the Baltic Sea by Using an Organic Rankine Cycle: A Case Study. Journal of Engineering for Gas Turbines and Power, 138(1), p. 011702.

[4] Franco, A. and Casarosa, C. (2014) Thermodynamic and heat transfer analysis of LNG energy recovery for power production. *Journal of Physics: Conference Series*, 547, p. 012012.

[5] Chen, H., Goswami, D., and Stefanakos, E. (2010) A review of thermodynamic cycles and working fluids for the conversion of low-grade heat. *Renewable and Sustainable Energy Reviews*, 14(9), pp. 3059-3067.

[6] Kim, K., Oh, J., and Kim, S. (2013) Analysis of Regenerative Power Cycle Utilizing Low-Grade Heat Source and LNG Cold Energy. *Mining, Metallurgy & Mechanical Engineering*, 1(5), pp. 291-295.

[7] Kim, M. (2004) Fundamental process and system design issues in CO2 vapor compression systems. *Progress in Energy and Combustion Science*, 30(2), pp. 119-174.

[8] Mago, P., Chamra, L., Srinivasan, K., and Somayaji, C. (2008) An examination of regenerative organic Rankine cycles using dry fluids. *Applied Thermal Engineering*, 28(8-9), pp. 998-1007.

[9] The Wärtsilä Gas Valve Unit Enclosed Design GVU-ED for marine applications (2017) [Online]. Available at: https://www.wartsila.com/twentyfour7/in-detail/the-wartsila-gas-valve-unit-enclosed-design-gvu-ed-for-marine-applications(2017).

[10] Zoglia,P. (2013).*Gas storage and supply systems.* Wartsila

[11] Software, S. (2017) LMS Imagine.Lab Amesim: Siemens PLM Software. Available at: https://www.plm.automation.siemens.com/en/products/lms/imagine-lab/amesim/.

[12] Lee, H. and Kim, K. (2015) Energy and Exergy Analyses of a Combined Power Cycle Using the Organic Rankine Cycle and the Cold Energy of Liquefied Natural Gas. Entropy, 17(9), pp. 6412-6432.

[13] Frangopoulos, C. (2009) Exergy, energy system analysis, and optimization. Oxford, Uinited Kingdom: Eolss Publishers Co. Ltd.

[14] El-Emam, R. and Dincer, I. (2013) Exergy and exergoeconomic analyses and optimization of geothermal organic Rankine cycle. Applied Thermal Engineering, 59(1-2), pp. 435-444.

[15] Grljušić, M., Medica, V., and Radica, G., Calculation of Efficiencies of a Ship Power Plant Operating with Waste Heat Recovery through Combined Heat and Power Production. Energies, 8(5), 4273-4299 (2015).

[16] Kakaç, S., Liu, H., and Pramuanjaroenkij, A. (2012) Heat Exchangers. Hoboken: CRC Press.

[17] James R. Couper; W. Roy Penney, James R. Fair, Stanley M. Walas, Chemical Process Equipment: selection and design, Elsevier Inc., 2nd ed. 2005.

[18] Tsatsaronis, G. and Cziesla, F. (2017) EXERGY, ENERGY SYSTEM ANALYSIS AND OPTIMIZATION. 1st edn. [Online]. ©Encyclopedia of Life Support Systems(EOLSS).Available at: https://www.eolss.net/samplechapters/C08/E3-19-01-02.pdf.

[19] Kern, D. (1983) Process heat transfer. Auckland: Mac Graw Hill.

[20] Engineering Page > Heat Exchangers > Typical Fouling Factors (2017) [Online]. 2017. Available at: http://www.engineeringpage.com/technology/thermal/fouling_factors.html

[21] Van Der Geld, C., Ganzevles, F., Simons, C., and Weitz, F., Geometry adaptations to improve the performance of compact polymer heat exchangers, Transactions IChemE: Part A, 79, 357–362, 2001.

[22] Harris, C., Kelly, K., Wang, T., McCandless, A., and Motakef, S., Fabrication, modeling and testing of micro-cross flow heat exchangers, Journal of Microelectromechanical Systems, 11, 726–735, 2002.

[23] Saman, W. and Alizadeh, S., Modeling and performance analysis of a cross-flow type plate heat exchanger for dehumidification/cooling, Solar Energy, 70(4), 361–372, 2001.

[24] Deronzier, J. C., and Bertolini, G. Plate heat exchanger in liquid crystal polymer, Applied Thermal Engineering, 17, 799–808, 1997.

[25] Macchi, E. and Astolfi, M., Organic rankine cycle (ORC) power systems. Elsevier Ltd, 1st edn, 70-75 (2016).

[26] Imran, M., Usman, M., Lee, D., and Park, B. (2015) THERMOECONOMIC ANALYSIS OF ORGANIC RANKINE CYCLE USING ZEOTROPIC MIXTURES. Brussels.

[27] Heberle, F. and Brüggemann, D. (2015) Thermo-Economic Evaluation of Organic Rankine Cycles for Geothermal Power Generation Using Zeotropic Mixtures. Energies, 8(3), pp. 2097-2124.

[28] Imran, M., Usman, M., Park, B., and Yang, Y. (2016) Comparative assessment of Organic Rankine Cycle integration for low temperature geothermal heat source applications. Energy, 102, pp. 473-490.

[29] Yang, F., Zhang, H., Song, S., Bei, C., Wang, H., and Wang, E. (2015) Thermoeconomic multi-objective optimization of an organic Rankine cycle for exhaust waste heat recovery of a diesel engine. Energy, 93, pp. 2208-2228.

[30] Han, Z., Li, P., Han, X., Mei, Z., and Wang, Z. (2017) Thermo-Economic Performance Analysis of a Regenerative Superheating Organic Rankine Cycle for Waste Heat Recovery. Energies, 10(10), p. 1593.

[31] Turton, R., Bailie, R., Whiting, W., and Shaeiwitz, J. (2009) Analysis, synthesis, and design of chemical processes. Estados Unidos: Pearson Education, Inc.

[32] Costall, A., Gonzalez Hernandez, A., Newton, P., and Martinez-Botas, R. (2015) Design methodology for radial turbo expanders in mobile organic Rankine cycle applications. Applied Energy, 157, pp. 729-743.

[33] Japan Liquefied Natural Gas Import Price (Monthly, USD per Million Btu) (2017). Available at:

http://ycharts.com/indicators/japan_liquefied_natural_gas_import_price.